Safety Factor Profile Control in Tokamaks via Feedback Linearization

Andres Pajares and Eugenio Schuster

***Abstract*— The tokamak is a torus-shaped machine in which a reactant ionized gas (plasma) is confined using magnetic fields for the purpose of generating energy from nuclear fusion reactions. In order to be commercially competitive, a tokamak needs to operate for long periods of time at high-performance operating points. Those high-performance scenarios are characterized by a steady-state, stable plasma operation, which is closely related to a property of the plasma that is known as the safety factor, q. Therefore, control of the q profile is one of the crucial aspects to the success of tokamaks. Significant research has been carried out by the fusion community to find control algorithms for the q profile. Most of that previous work makes use of approximate linearization and linear control techniques. In the present work, we propose a nonlinear model-based controller for the regulation of the q profile using feedback linearization. This nonlinear control approach may be applicable to a greater range of operating conditions, and may be able to reject larger perturbations than previous linear controllers. The effectiveness of the controller is demonstrated via a simulation study based on a DIII-D scenario.**

I. Introduction

The main goal of a fusion reactor is to obtain energy from nuclear reactions between hydrogen isotopes (typically, deuterium (D) and tritium (T)). These two reactants must be heated to extremely high temperatures (~ 10 million degrees) so that their kinetic energy is high enough to overcome the Coulombic repulsion force that exists between them and to enable nuclear fusion. Such high temperatures result in the reactants being in a plasma state. In plasmas, ions and electrons are separated, what makes these particles capable of driving electrical current and interacting with magnetic fields. Such properties of plasmas motivate the development of magnetic-confinement devices like the tokamak [1]. In these devices, a high temperature plasma is confined by means of magnetic fields inside a fixed toroidal volume where the appropriate conditions for fusion to occur are maintained. Much work has been done to find high-performance operating scenarios characterized by magnetohydrodynamic (MHD) stability and steady-state operation. Such scenarios are closely related to the safety factor q [1]. This property of the plasma is a measure of the pitch of the magnetic field lines, and plays a fundamental role in plasma stability and fusion performance. Therefore, active control of the q profile to maintain a desired operation arises as a key issue that needs to be solved for the success of tokamak reactors as efficient means of producing energy.

This material is based upon work partly supported by the U.S. Department of Energy, Office of Science, Office of Fusion Energy Sciences, under award DE-SC0010661. A. Pajares (andres.pajares@lehigh.edu) and E. Schuster (schuster@lehigh.edu) are with the Department of Mechanical Engineering and Mechanics, Lehigh University, Bethlehem, PA 18015, USA.

Extensive research has been carried out in order to develop control algorithms for the regulation of the q profile in tokamaks. In [2], a linearized data-driven model has been used to synthesize a controller that is applicable to scenarios in which the data-driven model is representative. Different controllers based on first-principles-driven models have been proposed in [3], [4], [5], [6], [7], where model linearization or quasi-linearization techniques around a nominal operating point have been utilized. Other first-principles-driven model-based control design work has produced controllers based on Lyapunov control theory [8] and backstepping techniques [9]. However, even these pieces of work use plasma-response models that have been partially linearized.

In this work, a first-principles-driven, control-oriented model of the q-profile evolution for high-confinement plasmas [10] is used. Based on this model, a nonlinear control algorithm using feedback linearization [11] is proposed. The main novelty of the proposed controller is that it is not based on a linearized approximation of the nonlinear model. Instead, the fact that the system is feedback linearizable is exploited, i.e., the nonlinear model is algebraically transformed into a linear model by means of a state-space transformation and a suitable choice of the control inputs. Feedback linearization allows for using linear control techniques once the nonlinear model is transformed into a linear model. The controller is capable of driving the system between considerably different operating points, while linear controllers are designed to work in a neighborhood of a nominal operating point. Also, the controller stabilizes the system even in the presence of large perturbations that drive the system away from the nominal operating point, where approximately linearized models may loose validity and model-based linear controllers may exhibit poor performance.

This work is organized as follows. A model for the q-profile evolution is introduced in Section II. This model is spatially discretized by using the finite-differences method in Section III. The feedback-linearized model is derived in Section IV. The control law is stated in Section V. Some simulation results are shown in Section VI to illustrate the controller performance. Finally, a summary and some conclusions are stated in Section VII.

II. Safety Factor Evolution Model

Magnetic field lines are normally closed in tokamaks and confine the plasma in a torus. They describe helical paths followed by the particles due to the Lorentz force exerted on them, as shown in Fig. 1. The magnetic field is denoted as $\bar{B}$, and its two components are the toroidal ($\bar{B}_\phi$) and poloidal ($\bar{B}_\theta$) magnetic fields. The magnetic-flux surfaces

are defined by all the points P that have the same poloidal magnetic flux, $\Psi = \int_S \bar{B}_\theta \cdot dS$, where S is the horizontal surface bounded by the toroidal ring passing through the point P. The axisymmetry provided by the toroidal geometry together with the selection of a spatial coordinate indexing the nested magnetic-flux surfaces (shown in Fig. 2) reduces the three-dimensional problem to just one dimension. The mean effective minor radius, ρ, is used to index each magnetic-flux surface. It is related to the toroidal magnetic flux, Φ, and to the vacuum toroidal magnetic field at the geometric major radius R_0 of the tokamak, $B_{\phi,0}$, by means of $\pi B_{\phi,0}\rho^2 = \Phi$. The mean effective minor radius can be normalized as $\hat{\rho} = \rho/\rho_\mathrm{b}$, where ρ_b is the value of ρ at the last closed magnetic-flux surface. The q profile is related to the spatial gradient of ψ as

$$q(\hat{\rho},t) = \frac{d\Phi}{d\Psi} = -\frac{d\Phi}{2\pi d\psi} = -\frac{B_{\phi,0}\rho_\mathrm{b}^2\hat{\rho}}{\partial\psi/\partial\hat{\rho}}, \tag{1}$$

where t is the time and $\psi(\hat{\rho},t)$ is the poloidal stream function, which is closely related to the poloidal flux, i.e., $\Psi = 2\pi\psi$. The evolution of the poloidal magnetic flux can be described by the magnetic diffusion equation [12],

$$\frac{\partial\psi}{\partial t} = \frac{\eta(T_\mathrm{e})}{\mu_0\rho_\mathrm{b}^2\hat{F}^2}\frac{1}{\hat{\rho}}\frac{\partial}{\partial\hat{\rho}}\left(\hat{\rho}D_\psi\frac{\partial\psi}{\partial\hat{\rho}}\right) + R_0\hat{H}\eta(T_\mathrm{e})\frac{\langle\bar{j}_\mathrm{NI}\cdot\bar{B}\rangle}{B_{\phi,0}}, \tag{2}$$

where $\eta(T_\mathrm{e})$ is the plasma resistivity, $T_\mathrm{e}(\hat{\rho},t)$ is the electron temperature, μ_0 is the vacuum permeability, $D_\psi(\hat{\rho}) = \hat{F}(\hat{\rho})\hat{G}(\hat{\rho})\hat{H}(\hat{\rho})$, where $\hat{F}$, $\hat{G}$, and $\hat{H}$ are spatially varying geometric factors pertaining to the magnetic configuration of a particular plasma equilibrium [13], $\bar{j}_\mathrm{NI}$ is the noninductive

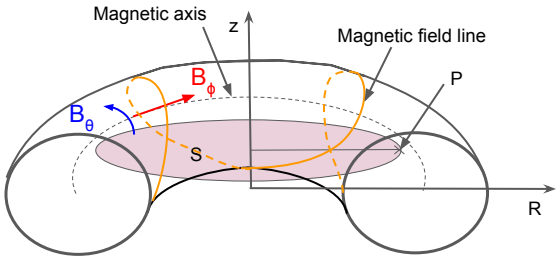

Fig. 1. Magnetic field configuration in a tokamak. The surface S normal to the z axis is used to compute the poloidal magnetic flux Ψ at point P.

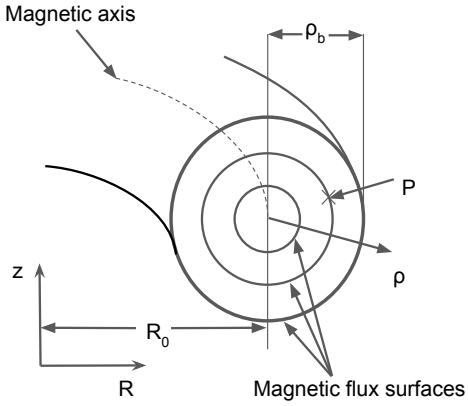

Fig. 2. Magnetic flux surfaces in a tokamak. Each magnetic flux surface is characterized by a constant poloidal magnetic flux.

current density from various sources and $\langle\cdot\rangle$ denotes the flux-surface average of a quantity. The boundary conditions are

$$\left.\frac{\partial\psi}{\partial\hat{\rho}}\right|_{\hat{\rho}=0} = 0, \quad \left.\frac{\partial\psi}{\partial\hat{\rho}}\right|_{\hat{\rho}=1} = -\frac{\mu_0}{2\pi}\frac{R_0}{\hat{G}|_{\hat{\rho}=1}\hat{H}|_{\hat{\rho}=1}}I_\mathrm{p}(t), \tag{3}$$

where $I_\mathrm{p}(t)$ is the total plasma current.

Control-oriented models [10] for the electron density, electron temperature, plasma resistivity and noninductive current density are used in this work. The electron density, $n_\mathrm{e}(\hat{\rho},t)$, is modeled as

$$n_\mathrm{e}(\hat{\rho},t) = n_\mathrm{e}^\mathrm{prof}(\hat{\rho})u_\mathrm{n}(t), \tag{4}$$

where $n_\mathrm{e}^\mathrm{prof}(\hat{\rho})$ is a reference profile and $u_\mathrm{n}(t)$ is the line-averaged electron density.

The electron temperature, $T_\mathrm{e}(\hat{\rho},t)$, is given by

$$T_\mathrm{e}(\hat{\rho},t) = k_{T_\mathrm{e}}(\hat{\rho})T_\mathrm{e}^\mathrm{prof}(\hat{\rho})I_\mathrm{p}(t)^\gamma P_\mathrm{tot}(t)^\epsilon n_\mathrm{e}(\hat{\rho},t)^\zeta, \tag{5}$$

where $k_{T_\mathrm{e}}(\hat{\rho})$ is a time-constant profile, $T_\mathrm{e}^\mathrm{prof}(\hat{\rho})$ is a reference profile, $P_\mathrm{tot}(t)$ is the total power injected to the plasma (see its definition below), and the parameters γ, ϵ and ζ are constants that describe how $T_\mathrm{e}(\hat{\rho},t)$ scales with $I_\mathrm{p}(t)$, $P_\mathrm{tot}(t)$ and $n_\mathrm{e}(\hat{\rho},t)$. In this work, it is assumed that $T_\mathrm{e}(\hat{\rho},t)$ scales with $I_\mathrm{p}(t)$, $P_\mathrm{tot}(t)$ and $n_\mathrm{e}(\hat{\rho},t)$ in the same way inside and outside the plasma core [1].

The plasma resistivity, $\eta(T_\mathrm{e})$, is given by

$$\eta(\hat{\rho},t) = \frac{k_\mathrm{sp}(\hat{\rho})Z_\mathrm{eff}}{T_\mathrm{e}^{3/2}(\hat{\rho},t)}, \tag{6}$$

where $k_\mathrm{sp}(\hat{\rho})$ is a time-constant profile, and Z_eff is the effective atomic number of the ions in the plasma, which is assumed constant and independent of the spatial coordinate.

Two sources of noninductive current are considered, the current injected by auxiliary sources (electron-cyclotron launchers, neutral beam injectors, etc.), and the self-generated bootstrap current. Therefore, $\bar{j}_\mathrm{NI}$ is expressed as $\bar{j}_\mathrm{NI}(\hat{\rho},t) = \sum_{i=1}^{N_\mathrm{aux}}\bar{j}_{\mathrm{aux},i}(\hat{\rho},t) + \bar{j}_\mathrm{BS}(\hat{\rho},t)$, where $\bar{j}_{\mathrm{aux},i}$ is the noninductive current density generated by the i-th auxiliary source for a total of N_aux auxiliary sources, and $\bar{j}_\mathrm{BS}$ is the noninductive current density produced by the bootstrap effect. The noninductive current density contribution of the i-th auxiliary source is modeled as

$$\frac{\langle\bar{j}_{\mathrm{aux},i}\cdot\bar{B}\rangle}{B_{\phi,0}} = j_{\mathrm{aux},i}^\mathrm{prof}(\hat{\rho})\frac{T_\mathrm{e}(\hat{\rho},t)^{\delta_i}}{n_\mathrm{e}(\hat{\rho},t)}P_{\mathrm{aux},i}(t), \tag{7}$$

where $j_{\mathrm{aux},i}^\mathrm{prof}(\hat{\rho})$ is a reference profile for the noninductive current density deposition, δ_i is a constant related to the current-drive efficiency, and $P_{\mathrm{aux},i}$ is the injected power. The bootstrap current contribution is modeled in this work as [14]

$$\frac{\langle\bar{j}_\mathrm{BS}\cdot\bar{B}\rangle}{B_{\phi,0}} = \frac{R_0}{\hat{F}}\left(\frac{\partial\psi}{\partial\hat{\rho}}\right)^{-1}\Big[2\mathcal{L}_{31}(\hat{\rho})T_\mathrm{e}(\hat{\rho},t)\frac{\partial n_\mathrm{e}(\hat{\rho},t)}{\partial\hat{\rho}} + \big(2\mathcal{L}_{31}(\hat{\rho}) + \mathcal{L}_{32}(\hat{\rho}) + \alpha(\hat{\rho})\mathcal{L}_{34}(\hat{\rho})\big)n_\mathrm{e}(\hat{\rho},t)\frac{\partial T_\mathrm{e}(\hat{\rho},t)}{\partial\hat{\rho}}\Big], \tag{8}$$

where the time-constant profiles $\alpha(\hat{\rho})$, $\mathcal{L}_{31}(\hat{\rho})$, $\mathcal{L}_{32}(\hat{\rho})$ and $\mathcal{L}_{34}(\hat{\rho})$ depend on the magnetic equilibrium configuration.

The total injected power is expressed as $P_{\text{tot}}(t) = \sum_{i=1}^{i=N_{\text{aux}}} P_{\text{aux,i}}(t) + P_{\text{ohm}}(t) - P_{\text{rad}}(t) + P'_{\text{fus}}(t)$, where $P_{\text{ohm}}(t)$ is the ohmic heating power, $P_{\text{rad}}(t)$ is the radiated power and $P'_{\text{fus}}(t)$ is the part of the fusion power that remains in the plasma. The ohmic heating power is given by $P_{\text{ohm}}(t) = \mathcal{R}_p(t) I_{\text{p}}(t)^2$, where $\mathcal{R}_p(t)$ is the total plasma resistance. The radiated power is modeled as $P_{\text{rad}}(t) = \int_0^1 Q_{\text{rad}}(\hat{\rho}, t) \frac{dV}{d\hat{\rho}} d\hat{\rho}$, where $Q_{\text{rad}} = k_{\text{brem}} Z_{\text{eff}}\, n_{\text{e}}(\hat{\rho}, t)^2 \sqrt{T_{\text{e}}(\hat{\rho}, t)}$, V is the volume enclosed by a magnetic surface within the plasma, and k_{brem} is the Bremsstrahlung radiation coefficient. In burning plasmas, the fusion power also contributes to the total injected power. Such contribution is modeled as $P'_{\text{fus}}(t) = \int_0^1 Q'_{\text{fus}}(\hat{\rho}, t) \frac{dV}{d\hat{\rho}} d\hat{\rho}$, where $Q'_{\text{fus}}(\hat{\rho}, t) = Q_\alpha n_{\text{D}}(\hat{\rho}, t) n_{\text{T}}(\hat{\rho}, t) \langle \sigma\nu \rangle_{\text{DT}}$, where Q_α = 3.52 MeV, $n_{\text{D}}(\hat{\rho}, t)$ and $n_{\text{T}}(\hat{\rho}, t)$ are the D and T densities, respectively, that are related to the electron density by the quasi-neutrality condition, $n_{\text{e}}(\hat{\rho}, t) \approx 2 n_{\text{D}}(\hat{\rho}, t) \approx 2 n_{\text{T}}(\hat{\rho}, t)$ (assuming 50:50 D-T mix), and $\langle \sigma\nu \rangle_{\text{DT}}$ is the D-T reactivity, which is a nonlinear function of the D-T temperature [15], that is assumed to be the same as T_{e}.

The magnetic diffusion equation (2) and the boundary conditions (3) can be rewritten as

$$\frac{\partial \psi}{\partial t} = \frac{f_\eta}{\hat{\rho}} \frac{\partial}{\partial \hat{\rho}} \left(\hat{\rho} D_\psi \frac{\partial \psi}{\partial \hat{\rho}} \right) u_\eta + \sum_{i=1}^{N_{\text{aux}}} f_{\text{aux},i} u_{\text{aux},i} + f_{\text{BS}} \left(\frac{\partial \psi}{\partial \hat{\rho}} \right)^{-1} u_{\text{BS}}, \quad (9)$$

$$\left. \frac{\partial \psi}{\partial \hat{\rho}} \right|_{\hat{\rho}=0} = 0, \; \left. \frac{\partial \psi}{\partial \hat{\rho}} \right|_{\hat{\rho}=1} = -k_{I_{\text{p}}} I_{\text{p}}, \quad (10)$$

where, just to simplify notation, the time and space dependencies have been dropped. In (9), f_η, $f_{\text{aux},i}$ and f_{BS} are functions of $\hat{\rho}$ and their shape is determined by the reference profiles and spatial functions introduced in (5)–(4). Also, in (10), $k_{I_{\text{p}}} = \mu_0 R_0 / (2\pi \hat{G}(1) \hat{H}(1))$. The time dependent functions u_η, $u_{\text{aux},i}$ and u_{BS}, written as

$$\begin{aligned} u_\eta &= I_{\text{p}}^{-3\gamma/2} P_{\text{tot}}^{-3\epsilon/2} u_{\text{n}}^{-3\zeta/2}, \\ u_{\text{aux},i} &= I_{\text{p}}^{\gamma(\delta_i - 3/2)} P_{\text{tot}}^{\epsilon(\delta_i - 3/2)} u_{\text{n}}^{\zeta(\delta_i - 3/2) - 1} P_{\text{aux},i}, \\ u_{\text{BS}} &= I_{\text{p}}^{-\gamma/2} P_{\text{tot}}^{-\epsilon/2} u_{\text{n}}^{1-\zeta/2}, \end{aligned} \quad (11)$$

are the "virtual" inputs to the system. Defining the poloidal flux gradient profile, θ, as

$$\theta(\hat{\rho}, t) \triangleq \frac{\partial \psi}{\partial \hat{\rho}}(\hat{\rho}, t), \quad (12)$$

we can express q in (1) in terms of θ as

$$q(\hat{\rho}, t) = -\frac{B_{\phi,0} \rho_{\text{b}}^2 \hat{\rho}}{\theta(\hat{\rho}, t)}. \quad (13)$$

Taking derivative with respect to $\hat{\rho}$, (9) can be rewritten as

$$\frac{\partial \theta}{\partial t} = \left[\frac{f_\eta}{\hat{\rho}} \frac{\partial \left(\hat{\rho} D_\psi \theta \right)}{\partial \hat{\rho}} \right]' u_\eta + \sum_{i=1}^{N_{\text{aux}}} f'_{\text{aux},i} u_{\text{aux},i} + \left[\frac{f_{\text{BS}}}{\theta} \right]' u_{\text{BS}}, \quad (14)$$

where the definition of θ in (12) is used and, to simplify notation, $(\cdot)' \triangleq \partial / \partial \hat{\rho}$. The boundary conditions become

$$\theta|_{\hat{\rho}=0} = 0, \quad \theta|_{\hat{\rho}=1} = -k_{I_{\text{p}}} I_{\text{p}}. \quad (15)$$

The first term in (14), related to u_η, can be written after application of the chain rule several times as $\left[\frac{f_\eta}{\hat{\rho}} \frac{\partial (\hat{\rho} D_\psi \theta)}{\partial \hat{\rho}} \right]' = h_{\text{diff},3} \theta + h_{\text{diff},2} \theta' + h_{\text{diff},1} \theta''$, where $h_{\text{diff},1} = f_\eta D_\psi$, $h_{\text{diff},2} = f_\eta \left(\frac{D_\psi}{\hat{\rho}} + 2 D'_\psi \right) + f'_\psi D_\psi$, and $h_{\text{diff},3} = f_\eta \left(D''_\psi + \frac{\hat{\rho} D'_\psi - D_\psi}{\hat{\rho}^2} \right) + f'_\eta \left(\frac{D_\psi}{\hat{\rho}} + D'_\psi \right)$. The last term in (14) can be expressed as $\left[\frac{f_{\text{BS}}}{\theta} \right]' = h_{\text{BS},1} \frac{1}{\theta} - h_{\text{BS},2} \frac{\theta'}{\theta^2}$, where $h_{\text{BS},1} = f'_{\text{BS}}$ and $h_{\text{BS},2} = f_{\text{BS}}$. By denoting $h_{\text{aux},i} = f'_{\text{aux},i}$, (14) can finally be rewritten as

$$\frac{\partial \theta}{\partial t} = (h_{\text{diff},1} \theta'' + h_{\text{diff},2} \theta' + h_{\text{diff},3} \theta) u_\eta + \sum_{i=1}^{N_{\text{aux}}} h_{\text{aux},i} u_{\text{aux},i} + \left(h_{\text{BS},1} \frac{1}{\theta} - h_{\text{BS},2} \frac{\theta'}{\theta^2} \right) u_{\text{BS}}. \quad (16)$$

III. Spatial Discretization of the Safety Factor Evolution Model

The finite-differences method is used to discretize (16) in the spatial domain, $\hat{\rho} \in [0, 1]$. The number of nodes is denoted as $N + 1$, and the values of θ at the nodes are denoted as θ_m, where $m = 0, 1, ..., N$. After discretization, the original partial differential equation (16) is transformed into a set of ordinary differential equations (ODE) given by

$$\begin{aligned} \dot{\theta}_m = &\left[h^m_{\text{diff},1} \frac{\theta_{m+1} + \theta_{m-1} - 2\theta_m}{\Delta \hat{\rho}^2} + h^m_{\text{diff},2} \frac{\theta_{m+1} - \theta_{m-1}}{2\Delta \hat{\rho}} + h^m_{\text{diff},3} \theta_m \right] u_\eta + \sum_{i=1}^{i=N_{\text{aux}}} h^m_{\text{aux},i} u_{\text{aux},i} \\ &+ \left[\frac{h^m_{\text{BS},1}}{\theta_m} - \frac{h^m_{\text{BS},2}}{\theta_m^2} \frac{\theta_{m+1} - \theta_{m-1}}{2\Delta \hat{\rho}} \right] u_{BS}, \end{aligned} \quad (17)$$

for $m = 1, 2, ..., N-1$, where $\Delta \hat{\rho} = 1/N$, and $\dot{\theta}_m$ and $h^m_{(\cdot)}$ denote the values of $\partial \theta / \partial t$ and $h_{(\cdot)}$, respectively, when evaluated at $\hat{\rho} = \hat{\rho}_m = m \Delta \hat{\rho}$. By introducing the terms $\alpha_m = h^m_{\text{diff},3} - 2 h^m_{\text{diff},1} / \Delta \hat{\rho}^2$, $\beta_m = h^m_{\text{diff},1} / \Delta \hat{\rho}^2 + h^m_{\text{diff},2} / (2\Delta \hat{\rho})$, and $\gamma_m = h_{\text{diff},1} / \Delta \hat{\rho}^2 - h_{\text{diff},2} / (2\Delta \hat{\rho})$, (17) is rewritten as

$$\begin{aligned} \dot{\theta}_m = &\left[\gamma_m \theta_m + \beta_m \theta_{m+1} + \alpha_m \theta_{m-1} \right] u_\eta + \sum_{i=1}^{i=N_{\text{aux}}} h^m_{\text{aux},i} u_{\text{aux},i} \\ &+ \left[\frac{h^m_{\text{BS},1}}{\theta_m} - \frac{h^m_{\text{BS},2}}{\theta_m^2} \frac{\theta_{m+1} - \theta_{m-1}}{2\Delta \hat{\rho}} \right] u_{BS}. \end{aligned} \quad (18)$$

Using the introduced notation, the boundary conditions become

$$\theta_0 = 0, \quad \theta_N = -k_{I_{\text{p}}} I_{\text{p}}. \quad (19)$$

IV. Feedback Linearization of the Discretized Safety Factor Evolution Model

The ODE system (18), together with the boundary conditions (19), compose the discretized nonlinear model for the q-profile evolution. It can be expressed in matrix form as

$$\dot{\hat{\theta}} = G(\hat{\theta})\, u = \sum_{j=1}^{j=3+N_{\text{aux}}} g_j(\hat{\theta}) u_j, \qquad \hat{y} = h(\hat{\theta}) = \hat{\theta}, \quad (20)$$

where $\hat{\theta} = [\theta_1, \theta_2, ..., \theta_{N-1}, \theta_N]^T \in \mathbb{R}^{N\times 1}$ is the state vector, $G(\hat{\theta}) \in \mathbb{R}^{N\times(3+N_{\text{aux}})}$, $u = [u_\eta, u_{\text{aux},1}, ..., u_{\text{aux},N_{\text{aux}}}, u_{BS}, \dot{I}_{\text{p}}]^T \in \mathbb{R}^{(3+N_{\text{aux}})\times 1}$ is the input vector, and $\hat{y}$ is the output vector. Also, $g_j(\hat{\theta})$ is the j-th column in $G(\hat{\theta})$ and u_j is the j-th component of u. Many tokamaks are gaining the capability of reconstructing $\theta(\hat{\rho}, t)$ at different spatial locations in real time. Then, it is assumed that $\hat{\theta}$ is measurable, and the output of the system is chosen to be the same as the state, as expressed in (20).

It can be said that the system (20) is feedback linearizable in a region $D \subset \mathbb{R}^{N\times 1}$ if and only if its associated vector relative degree, denoted as $r = (r_1, r_2, ..., r_N)$, is such that the sum of all its components fulfills $r_1 + r_2 + ... + r_N = N$, for all $\hat{\theta} \in D$. A state-space transformation $\hat{z} = T(\hat{\theta})$ and an input choice for u can be sought in this case to exactly linearize the system. From the definition of vector relative degree [11], it follows that $3 + N_{\text{aux}}$ must be equal to N, which implies that it is necessary to use a discretization grid with a number of nodes that is determined by the number of virtual inputs to the system. This condition makes $G(\hat{\theta})$ a square matrix. Moreover, also from the definition of the vector relative degree, it is found that $r_i = 1$, for $i = 1, 2, ..., N$, if and only if the matrix $A(\hat{\theta})$ given by

$$A(\hat{\theta}) = \begin{bmatrix} \mathcal{L}_{g_1}h_1(\hat{\theta}) & \mathcal{L}_{g_2}h_1(\hat{\theta}) & ... & \mathcal{L}_{g_N}h_1(\hat{\theta}) \\ \mathcal{L}_{g_1}h_2(\hat{\theta}) & \mathcal{L}_{g_2}h_2(\hat{\theta}) & ... & \mathcal{L}_{g_N}h_2(\hat{\theta}) \\ \vdots & \vdots & \ddots & \vdots \\ \mathcal{L}_{g_1}h_N(\hat{\theta}) & \mathcal{L}_{g_2}h_N(\hat{\theta}) & ... & \mathcal{L}_{g_N}h_N(\hat{\theta}) \end{bmatrix}, \quad (21)$$

is invertible for all $\hat{\theta} \in D$, where $h_i(\hat{\theta})$ is the j-th component of h, for $j = 1, ..., N$, $i = 1, ..., N$. Using the definition of Lie Derivative, and the output choice $\hat{y} = \hat{\theta}$,

$$\mathcal{L}_{g_j}h_i(\hat{\theta}) = \frac{\partial h_i(\hat{\theta})}{\partial \hat{\theta}} g_j(\hat{\theta}) = g_{ij}(\hat{\theta}), \quad (22)$$

i.e., $A(\hat{\theta}) = G(\hat{\theta})$, and it can be concluded that the system (20) is feedback linearizable if and only if $G(\hat{\theta})$ is invertible for all $\hat{\theta} \in D$. As $G(\hat{\theta})$ is square, $G(\hat{\theta})$ has to be a full rank matrix to be invertible. This depends, obviously, on the control capability of the auxiliary sources, that must have different enough deposition profiles $j^{\text{prof}}_{\text{aux},i}$ to allow for the control of N different nodes, i.e., the related functions $h_{\text{aux},i}$ must form linearly independent columns and add rank in $G(\hat{\theta})$. Also, the invertibility of $G(\hat{\theta})$ is subject to the diffusive and bootstrap related terms, which are functions of $h^m_{\text{diff},1}$, $h^m_{\text{diff},2}$, $h^m_{\text{diff},3}$, $h^m_{\text{BS},1}$ and $h^m_{\text{BS},2}$, and the state $\hat{\theta}$. Based on typical values of these functions, and the typical values of $\hat{\theta}$ found in tokamaks that define the region of interest D, it is found that DIII-D tokamak yields a model with invertible $G(\hat{\theta})$, and therefore a model which is feedback linearizable in such D. Due to the mildness of the required conditions, it is indeed reasonable to conclude that if a similar modeling approach is followed, most tokamak designs will also yield models that are feedback linearizable in D. Therefore, by choosing

$$u = G^{-1}(\hat{\theta})v, \quad (23)$$

the system (20) renders linear,

$$\dot{\hat{\theta}} = v, \qquad \hat{y} = \hat{\theta}, \quad (24)$$

with $\hat{z} = \hat{\theta}$ (i.e., the change of coordinates $\hat{z} = T(\hat{\theta})$ is just an identity transformation). (24) is an exactly, feedback-linearized version of (20) which is valid for all $\hat{\theta} \in D$.

V. Feedback Linearization Control Law

The control objective is to drive the system (20), or its feedback-linearized version (24), to a desired plasma state defined by a target q profile. This target q profile is related to a target θ profile by (13). This target θ profile is denoted as $\theta^{\text{ref}}(\hat{\rho}, t)$, and $\hat{\theta}^{\text{ref}}$ is a vector containing the N values of $\theta^{\text{ref}}(\hat{\rho}, t)$ at $\hat{\rho}_m = m\Delta\hat{\rho}$, for $m = 1, 2, ..., N$. By setting

$$v = -K_p\left((\hat{\theta} - \hat{\theta}^{\text{ref}}) + \frac{1}{T_i}\int_{t_0}^{t}(\hat{\theta} - \hat{\theta}^{\text{ref}})\, dt\right) + \dot{\hat{\theta}}^{\text{ref}}, \quad (25)$$

a state-feedback controller with design parameters K_p and T_i is used to control the feedback-linearized system (24). In (25), t is the current time and t_0 is the initial time. Plugging (25) into (23), the nonlinear control law for u is

$$u = -G^{-1}(\hat{\theta})\left[K_p\left((\hat{\theta} - \hat{\theta}^{\text{ref}}) + \frac{1}{T_i}\int_{t_0}^{t}(\hat{\theta} - \hat{\theta}^{\text{ref}})dt\right) + \dot{\hat{\theta}}^{\text{ref}}\right], \quad (26)$$

and defining an error vector as $e = \hat{\theta} - \hat{\theta}^{\text{ref}}$, the state equation in (24) becomes

$$\dot{e} = -K_p\left(e + \frac{1}{T_i}\int_{t_0}^{t} e\, dt\right). \quad (27)$$

This ensures that $e \to 0$ exponentially as $t \to \infty$, i.e., $\hat{\theta} \to \hat{\theta}^{\text{ref}}$ exponentially fast. So, if $\hat{\theta}$ is known at a particular time step, u can be computed from (26), and then the real inputs to the system can be obtained from (11), i.e., I_{p}, u_{n} and $P_{\text{aux},i}$ (for $i = 1, ..., N_{\text{aux}}$).

In real experiments, control of the electron density n_{e} is a quite challenging problem. Therefore, in order to reproduce real experiments with the highest possible accuracy in the simulation studies presented in this work, it is assumed that n_{e} is not controllable but measurable, what implies that $u_{\text{n}}(t)$ is not an input to the system, but just a known magnitude. It is important to note that the dimension of the "virtual" input vector u is $3 + N_{\text{aux}}$, while there are only $1 + N_{\text{aux}}$ real inputs (I_{p} and $P_{\text{aux},i}$, for $i = 1, ..., N_{\text{aux}}$). Also, the actuators have physical constraints. Thus, in general, it is not possible to reach any "virtual" input vector u with the existing real inputs to the system, i.e., the system is overconstrained. To deal with this problem, the nonlinear least-squares method is utilized to find the values of I_{p}, $P_{\text{aux},1}$,..., $P_{\text{aux},N_{\text{aux}}}$ that minimize the quadratic error of the nonlinear set of equations

$$u + G^{-1}(\hat{\theta})\left[K_p\left(e + \frac{1}{T_i}\int_{t_0}^{t} e\, dt\right) + \dot{\hat{\theta}}^{\text{ref}}\right] = 0,$$

where $u = u(I_{\text{p}}, P_{\text{aux},1}, ..., P_{\text{aux},N_{\text{aux}}}) \in \mathbb{R}^{(3+N_{\text{aux}})\times 1}$ is the nonlinear function given by (11). More details about the nonlinear least-squares method can be found in [16].

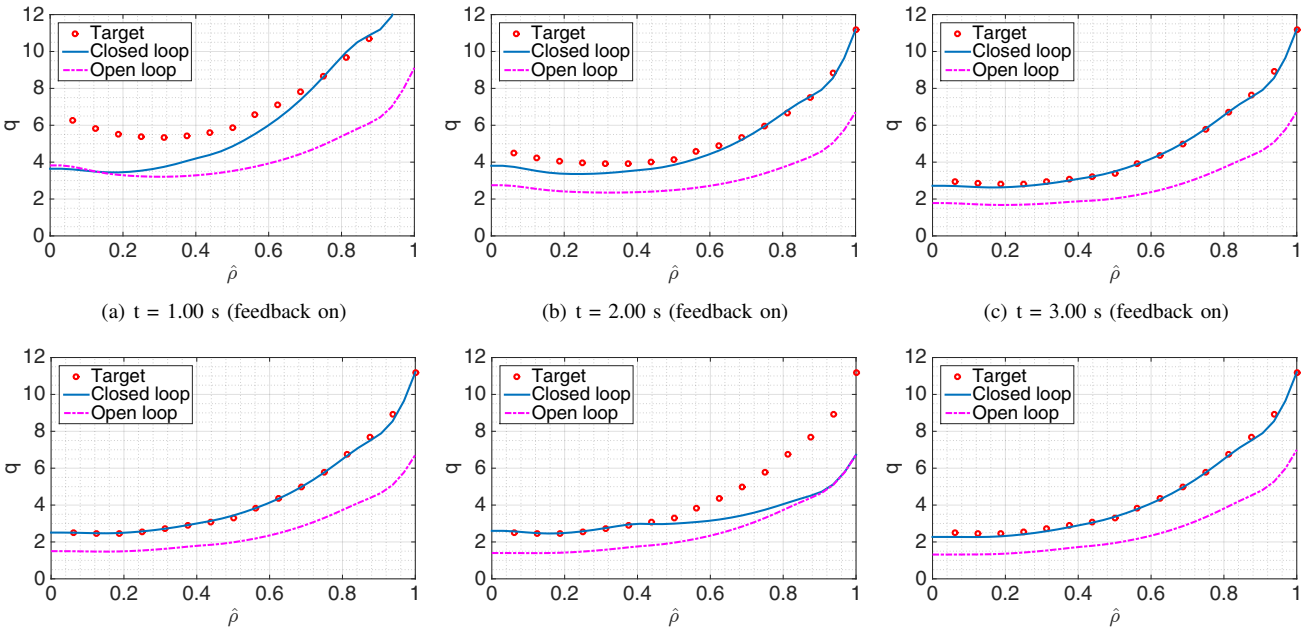

(a) t = 1.00 s (feedback on) (b) t = 2.00 s (feedback on) (c) t = 3.00 s (feedback on)

(d) t = 4.25 s (feedback on) (e) t = 4.75 s (feedback off) (f) t = 5.90 s (feedback on)

Fig. 3. Comparison of q profiles at various times for the target profile (red circular markers), the closed-loop simulation (blue solid) and open-loop simulation (magenta dashed-dotted). The effect of turning off the controller can be noted in (e). Track recovery of the target profile by turning the feedback controller back on can be appreciated in (f).

VI. Simulation Results in a DIII-D Scenario

In this section, the control law (26) is tested through simulations based on the model described in Section II. The reference profiles and spatial functions ($\hat{F}$, $\hat{G}$, $\hat{H}$, k_{T_e}, k_{sp}, $j^{\text{prof}}_{\text{aux},i}$, $\mathcal{L}_{31}$, $\mathcal{L}_{32}$, $\mathcal{L}_{34}$, α and $n^{\text{prof}}_{\text{e}}$) used in the simulations correspond to a particular DIII-D scenario [10]. However, it must be noted that the controller synthesis is independent of the scenario used for this simulation study. For the temperature model, based on experimental T_{e} evolution, γ = 1, ϵ = 0.5 and ζ = -1 are chosen. The other constants of the model are taken as $B_{\phi,0}$ = 1.65 T, R_0 = 1.69 m, ρ_b = 0.82 m and Z_{eff} = 1.75. The DIII-D auxiliary sources considered in this work are 6 electron cyclotrons (EC) and 7 neutral beam injectors (NBI), i.e., $N_{\text{EC}} = 6$, $N_{\text{NBI}} = 7$ and N_{aux} = 13, and their efficiency is taken as $\delta_i = 1$ for EC's and $\delta_i = 0.5$ for NBI's. Each EC power is denoted as as $P_{\text{EC},i}$, for $i = 1, ..., 6$, and each NBI power as $P_{\text{NBI},i}$, for $i = 1, ..., 7$. The maximum power achievable by each EC is 0.5 MW, while the maximum power achievable by each NBI is 2 MW. It is also considered that $P'_{\text{fus}}(t)$ can be neglected, as the plasma in DIII-D (and in any other present tokamak) does not produce a significant amount of fusion power.

A set of simulations is executed with the purpose of testing the reference tracking capability of the controller. First, a feedforward-only (open-loop) simulation is run with the input trajectories and initial conditions achieved in DIII-D shot 150320. For the closed-loop simulation study a target q profile is created by modifying the nominal q-profile evolution obtained in the feedforward-only simulation. When $t \in [0.5, 4]$ s, the target q profile is chosen around 65% larger than the nominal q profile obtained in the feedforward-only simulation, and after t = 4 s, the target q profile is held constant in time. By keeping the target q profile constant after t = 4 s, the controller is tested in an even more demanding situation because the target q profile is still further from the nominal open-loop q-profile evolution and it may not even be achievable due to the overconstrained nature of the system. Once the target q profile is computed, a feedforward + feedback (closed-loop) simulation is executed in which the controller attempts to drive the system to the target q profile. A comparison of the q-profile evolution in open loop (feedforward only) and closed loop (feedforward+feedback), together with the target q profile, is shown in Fig. 3. Time traces of q at various spatial locations are shown in Fig. 4, where also the open-loop, closed-loop and target q profiles are compared. Fig. 5 shows the evolution of the control inputs in both open-loop and closed-loop simulations. Good reference tracking is achieved in closed loop, despite using a target q profile which is considerably higher than the feedforward-only q profile. The controller is turned off at $t \in [4.25, 4.75]$ s (shaded region) to show how the system evolves with no control, and to test the controller capability to recover target tracking when it is turned on again at t = 4.75 s. It is found that the controller is able to recover target tracking with quite good performance after being turned on. It can be noted that the inner plasma region ($\hat{\rho} \leq 0.2$, approximately) is the one that shows a slower response to control actuation. This could be critical because the minimum q value, which plays a fundamental role in MHD stability, is normally found in such region. However, good reference tracking is also achieved for the inner region. It must be noted that the trajectory for the plasma current requires values of I_{p} that may be too low for operation in DIII-D or any other tokamak device. This is naturally

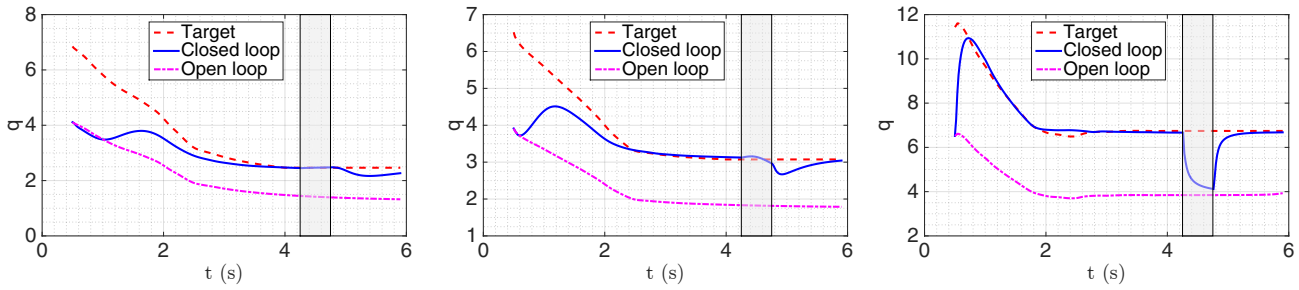

(a) $\hat{\rho} = 0.125$ (b) $\hat{\rho} = 0.500$ (c) $\hat{\rho} = 0.875$

Fig. 4. Time traces of q at various spatial points for the target profile (red dashed), the closed-loop simulation (blue solid) and open-loop simulation (magenta dashed-dotted). The effect of turning off the controller can be noted in between t = 4.25 s and t = 4.75 s (shaded region). Track recovery of the target profile by turning the controller back on can be appreciated after $t = 4.75$ s.

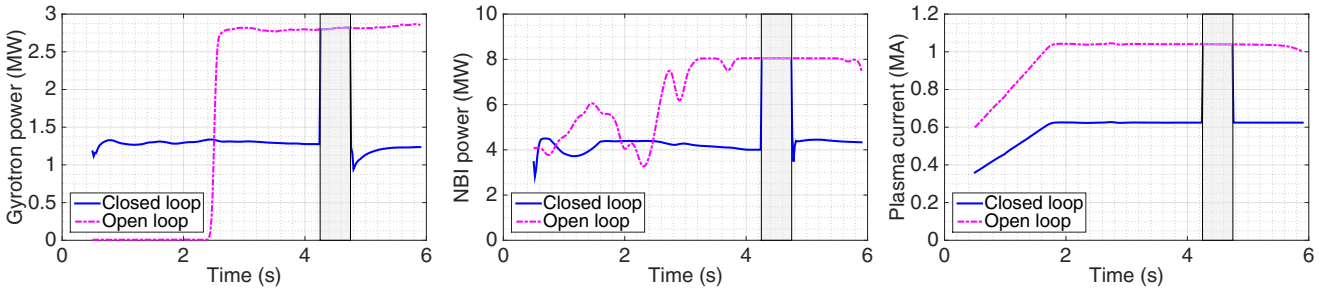

(a) Total EC power $\sum_{i=1}^{i=6} P_{\mathrm{EC},i}$ (b) Total NBI power $\sum_{i=1}^{i=7} P_{\mathrm{NBI},i}$ (c) Plasma current I_{p}

Fig. 5. Actuator trajectories during closed-loop (blue solid) and open-loop (magenta dashed-dotted) simulations. Note that the closed-loop and open-loop trajectories coincide between t = 4.25 s and t = 4.75 s (shaded region), as a result of turning off the feedback control. Also note that the value for $I_{\mathrm{p}}(t)$ may be unrealistic for operation in real devices as the result of choosing a probably non-physical target q-profile evolution for simulation-only purposes.

due to the fact that the target q profile is too demanding, with high values of q, specially at $\hat{\rho} \approx 1$. The choice of a demanding, probably non-physical, target q profile responds only to the purpose of showing the controller performance in simulations.

VII. Summary and Conclusions

A new control approach has been presented for the q-profile evolution in tokamaks. Using feedback linearization for the first time ever, the nonlinear model of the q-profile evolution has been transformed into a linear system which is valid in a region of interest D without approximately linearizing the model. By means of a simulation study for a DIII-D scenario, it has been demonstrated that this controller is able to drive the system between different target profiles that are considerably distant. Such performance may be difficult to match with previous linear controllers synthesized from approximately linearized models. Although the simulation study has been carried out for a high-confinement DIII-D scenario, the controller synthesis is independent of the scenario and the device.

References

[1] J. Wesson, *Tokamaks*. Oxford, UK: Clarendon Press, 1984.

[2] D. Moreau *et al.*, "Integrated magnetic and kinetic control of advanced tokamak plasmas on DIII-D based on data-driven models," *Nuclear Fusion*, vol. 53, no. 6, p. 063020, 2013.

[3] Y. Ou, C. Xu, E. Schuster, T. C. Luce, J. R. Ferron, M. L. Walker, and D. A. Humphreys, "Optimal tracking control of current profile in tokamaks," *IEEE Transactions on Control Systems Technology*, vol. 19, no. 2, 2011.

[4] J. Barton, M. Boyer, W. Shi, E. Schuster *et al.*, "Toroidal Current Profile Control During Low Confinement Mode Plasma Discharges in DIII-D via First-Principles-Driven Model-based Robust Control Synthesis," *Nuclear Fusion*, vol. 52, no. 123018, 2012.

[5] S. Kim and J. Lister, "A potentially robust plasma profile control approach for ITER using real-time estimation of linearized profile response models," *Nuclear Fusion*, vol. 52, p. 074002, 2012.

[6] M. Boyer, J. Barton, E. Schuster *et al.*, "First-Principles-Driven Model-Based Current Profile Control for the DIII-D Tokamak via LQI Optimal Control," *Plasma Physics and Controlled Fusion*, vol. 55, no. 105007, 2013.

[7] J. Barton, K. Besseghir, J. Lister, and E. Schuster, "Physics-based control-oriented modeling and robust feedback control of the plasma safety factor profile and stored energy dynamics in ITER," *Plasma Physics and Controlled Fusion*, vol. 57, no. 115003, 2015.

[8] F. Arogmendo *et al.*, "Lyapunov-based Distributed Control of the Safety-factor Profile in a Tokamak Plasma," *Nuclear Fusion*, vol. 53, no. 3, p. 033005, 2013.

[9] M. Boyer, J. Barton, E. Schuster, M. Walker, T. Luce, J. Ferron, B. Penaflor, R. Johnson, and D. Humphreys, "Backstepping Control of the Toroidal Plasma Current Profile in the DIII-D Tokamak," *Control Systems Technology, IEEE Transactions on*, vol. 22, no. 5, pp. 1725–1739, Sept 2014.

[10] J. Barton, W. Shi *et al.*, "Physics-based Control-oriented Modeling of the Current Density Profile Dynamics in High-performance Tokamak Plasmas," *52nd IEEE International Conference on Decision and Control*, 2013.

[11] A. Isidori, *Nonlinear Control Systems*. Berlin: Springer, 1995.

[12] F. Hinton and R. Hazeltine, "Theory of plasma transport in toroidal confinement systems," *Rev. Mod. Phys.*, vol. 48, pp. 239–308, 1976.

[13] Y. Ou, T. Luce, E. Schuster *et al.*, "Towards model-based current profile control at DIII-D," *Fusion Engineering and Design*, vol. 82, pp. 1153–1160, 2007.

[14] O. Sauter *et al.*, "Neoclassical conductivity and bootstrap current formulas for general axisymmetric equilibria and arbitrary collisionality regime," *Physics of Plasmas*, vol. 6, no. 7, p. 2834, 1999.

[15] L. M. Hively, "Convenient Computational Forms for Maxwellian Reactivities," *Nuclear Fusion*, vol. 17, no. 4, p. 873, 1977.

[16] G. A. F. Seber and C. J. Wild, *Nonlinear Regression*. Wiley-Interscience, Hoboken, NJ, 2003.